iScience

CellPress
OPEN ACCESS

Article

The transcription factor IRF4 determines the anti-tumor immunity of CD8$^+$ T cells

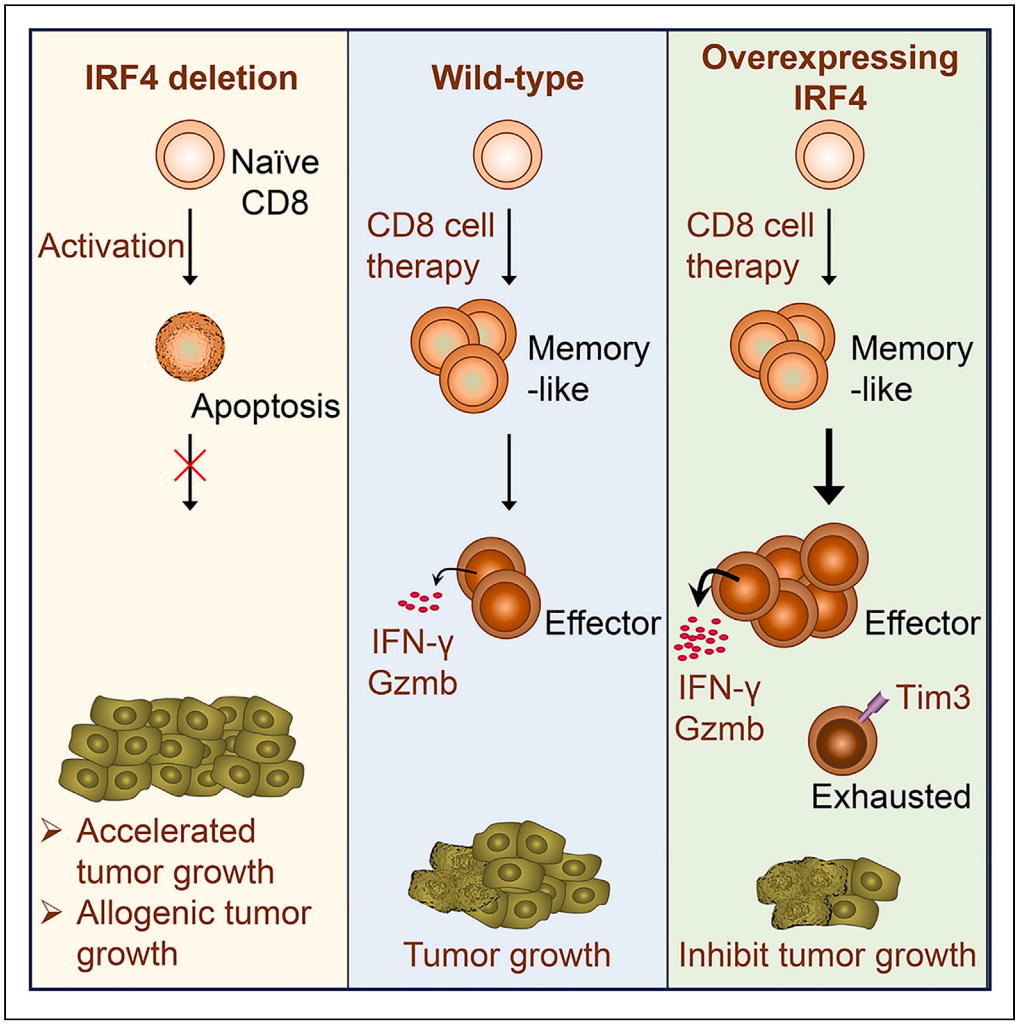

Hui Yan, Yulin Dai, Xiaolong Zhang, ..., Xian C. Li, Zhongming Zhao, Wenhao Chen

wchen@houstonmethodist.org

Highlights

T cells require IRF4 for anti-tumor immune response

Deleting IRF4 in T cells allows growth of subcutaneous allogeneic tumors

Overexpressing IRF4 in therapeutic T cells enhances their anti-tumor activity

IRF4-engineered T cell therapy boosts endogenous anti-tumor response

Yan et al., iScience *26*, 108087
November 17, 2023
https://doi.org/10.1016/j.isci.2023.108087

iScience

CellPress
OPEN ACCESS

Article

The transcription factor IRF4 determines the anti-tumor immunity of CD8$^+$ T cells

Hui Yan,[1,2] Yulin Dai,[3] Xiaolong Zhang,[1] Hedong Zhang,[1] Xiang Xiao,[1] Jinfei Fu,[1] Dawei Zou,[1] Anze Yu,[1] Tao Jiang,[1] Xian C. Li,[1,4] Zhongming Zhao,[3] and Wenhao Chen[1,4,5,*]

SUMMARY

Understanding the factors that regulate T cell infiltration and functional states in solid tumors is crucial for advancing cancer immunotherapies. Here, we discovered that the expression of interferon regulatory factor 4 (IRF4) was a critical T cell intrinsic requirement for effective anti-tumor immunity. Mice with T-cell-specific ablation of IRF4 showed significantly reduced T cell tumor infiltration and function, resulting in accelerated growth of subcutaneous syngeneic tumors and allowing the growth of allogeneic tumors. Additionally, engineered overexpression of IRF4 in anti-tumor CD8$^+$ T cells that were adoptively transferred significantly promoted their tumor infiltration and transition from a naive/memory-like cell state into effector T cell states. As a result, IRF4-engineered anti-tumor T cells exhibited significantly improved anti-tumor efficacy, and inhibited tumor growth either alone or in combination with PD-L1 blockade. These findings identify IRF4 as a crucial cell-intrinsic driver of T cell infiltration and function in tumors, emphasizing the potential of IRF4-engineering as an immunotherapeutic approach.

INTRODUCTION

T cells are essential in mediating anti-tumor immunity, and T cell-based immunotherapies are expected to become a crucial component of cancer therapy. Immune checkpoint blockade and adoptive transfer of genetically engineered T cells are two promising approaches.[1,2] Checkpoint blockade either activates pre-existing tumor-infiltrating T cells or attracts peripheral anti-tumor T cells into tumors.[3–5] However, this therapy's effectiveness is limited as it only benefits a fraction of cancer patients, depending on the presence and functional states of endogenous anti-tumor T cells.[3,4] In contrast, the efficacy of adoptive T cell therapy is less dependent on endogenous anti-tumor immunity. For example, in the treatment of hematologic malignancies, polyclonal T cells are used to produce chimeric antigen receptor (CAR) T cells, which are genetically engineered to target cancer cells.[2] Nevertheless, CAR T cell therapy currently has limited efficacy in eliminating solid tumors, highlighting the need to improve the biological function of genetically engineered T cells *in vivo*.

The activation and differentiation of T cells are primarily mediated by the AP-1, NFAT, and NF-κB transcription factor families.[6] Reduced NF-κB activity in T cells impairs the anti-tumor immune response,[7] while overexpressing c-Jun, an AP-1 transcription factor, in CAR T cells enhances their functionality against solid tumors.[8] Notably, BATF, a member of the AP-1 family, can also enhance CAR T cell expansion and effector function within tumors via its interaction with IRF4.[9] While NFAT drives T cell function, it can also promote dysfunction by inducing TOX and NR4A transcription factors.[10] Knocking out all three NR4A factors in CAR T cells promotes solid tumor repression.[11]

Interferon regulatory factor 4 (IRF4) is a member of the IRF family of transcription factors that is preferentially expressed in hematopoietic cells and governs many aspects of T cell, B-cell, and dendritic cell differentiation and function.[12–14] Upon antigen/TCR stimulation, *Irf4* is induced in T cells and plays a crucial role in translating TCR affinity into appropriate transcriptional programs.[15] IRF4 controls the differentiation of T helper (Th)2, Th9, Th17, T follicular helper, regulatory T (Treg), and cytotoxic effector CD8$^+$ T cells.[16–22] Ablation of IRF4 abrogates T cell immunity in microbial infection, allergy, autoimmunity, graft-versus-host reaction, and transplant rejection, as we and others have found.[12,18,21,23–26]

In this study, we investigated the role of IRF4 in anti-tumor T cell immunity. IRF4 deletion in T cells significantly accelerated subcutaneous syngeneic and allogeneic tumor growth and reduced T cell infiltration and function in tumors. Conversely, retroviral gene transduction to overexpress IRF4 in anti-tumor CD8$^+$ T cells significantly inhibited tumor growth upon adoptive transfer, either alone or in combination

[1]Immunobiology & Transplant Science Center, Department of Surgery, Houston Methodist Research Institute & Institute for Academic Medicine, Houston Methodist Hospital, Houston, TX 77030, USA
[2]Department of Medicine Oncology, The General Hospital of Ningxia Medical University, Yinchuan 750004, China
[3]Center for Precision Health, School of Biomedical Informatics, The University of Texas Health Science Center at Houston, Houston, TX 77030, USA
[4]Department of Surgery, Weill Cornell Medicine, Cornell University, New York, NY 10065, USA
[5]Lead contact
*Correspondence: wchen@houstonmethodist.org
https://doi.org/10.1016/j.isci.2023.108087

with PD-L1 blockade. IRF4-engineering in adoptively transferred anti-tumor CD8$^+$ T cells not only promoted their infiltration into tumors, but also their transition from a TCF1$^+$ naive/memory-like cell state into effector cell states, as shown by single-cell RNA sequencing (scRNA-seq) analysis. Furthermore, adoptive IRF4-engineered T cell therapy invigorated the endogenous CD8$^+$ T cell response in tumors. Our findings demonstrate that IRF4 is required for T cells to exert anti-tumor immunity and that IRF4-engineering holds promise for improving adoptive T cell therapy.

RESULTS

T cells depend on IRF4 to exert their anti-tumor immune response

We investigated the role of IRF4, a transcription factor that translates TCR signaling into proper T cell responses, in anti-tumor T cell immunity. Specifically, we aimed to determine whether ablation of IRF4 in T cells affects the growth of syngeneic and allogeneic tumors. Our findings revealed that T-cell–specific IRF4 deletion in mice (*Irf4*$^{fl/fl}$*Cd4-Cre*; B6 background) does not reduce peripheral T cell numbers.[26] To examine the impact of IRF4 ablation on syngeneic tumors, we subcutaneously injected B16-F10 melanoma or TRAMP-C1 prostate cancer cells into *Irf4*$^{fl/fl}$*Cd4-Cre* and wild type (WT) B6 mice (Figure 1A). We observed that all B16-F10 tumors in *Irf4*$^{fl/fl}$*Cd4-Cre* mice grew faster than those in WT B6 mice, resulting in significantly shortened survival of *Irf4*$^{fl/fl}$*Cd4-Cre* mice (Figure 1B). In addition, the proportion of CD4$^+$ and CD8$^+$ T cells in CD45$^+$ tumor infiltrating cells was significantly lower in *Irf4*$^{fl/fl}$*Cd4-Cre* mice compared to WT B6 mice, and their CD8$^+$ tumor infiltrating T cells expressed significantly less Ki-67 and IFN-γ (Figure 1C). A similar trend was observed in TRAMP-C1 tumor growth, where all tumors in *Irf4*$^{fl/fl}$*Cd4-Cre* mice were over 1390 mm^3 in size at the end of the study period, while all tumors in WT B6 mice were smaller than 570 mm^3 (Figure 1D). The CD4$^+$ and CD8$^+$ T cell frequencies in TRAMP-C1 tumors of the *Irf4*$^{fl/fl}$*Cd4-Cre* group were also significantly lower than those of the WT B6 group (Figure 1E); however, the mechanisms behind this observation remain unclear.

Furthermore, to determine the impact of IRF4 ablation on allogeneic tumors, we implanted CT26 colon carcinoma cells of BALB/c origin into BALB/c, WT B6, and *Irf4*$^{fl/fl}$*Cd4-Cre* mice (Figure 1A). We found that WT B6 mice completely prevented allogeneic CT26 tumor growth. In contrast, T-cell–specific IRF4 deletion in B6 mice (*Irf4*$^{fl/fl}$*Cd4-Cre*) allowed the growth of allogeneic CT26 tumors, which were comparable in size to those of the BALB/c mouse group (Figures 1F and 1G). Collectively, our study demonstrates that ablation of IRF4 in T cells abrogates their ability to control tumor growth, both in the context of syngeneic and allogeneic tumors.

IRF4 is necessary for the survival of anti-tumor CD8$^+$ T cells

TCR transgenic CD8$^+$ T cells from Pmel-1 mice recognize the melanoma-associated antigen gp100 and express the congenic marker Thy1.1. We examined how IRF4 deletion affects anti-tumor CD8$^+$ T cells by generating Thy1.1$^+$ *Irf4*$^{-/-}$ Pmel-1 and Thy1.1$^+$Thy1.2$^+$ WT Pmel-1 mice, which were used in a Pmel-1 T cell adoptive transfer model (Figures 2A and 2B). After co-injecting freshly isolated Thy1.1$^+$ *Irf4*$^{-/-}$ Pmel-1 and Thy1.1$^+$Thy1.2$^+$ WT Pmel-1 T cells into Thy1.2$^+$ WT B6 mice on the same day of B16-F10 implantation, we found that both types of cells were detected in spleens and draining lymph nodes (DLNs) at two weeks post-cell transfer. However, in B16-F10 tumors, the transferred Pmel-1 T cells were less present, especially the Thy1.1$^+$ *Irf4*$^{-/-}$ Pmel-1 T cells, which were barely detectable (Figure 2C). The percentages of *Irf4*$^{-/-}$ Pmel-1 T cells among total co-transferred Pmel-1 T cells in spleens, DLNs, and tumors were significantly lower than those of WT Pmel-1 T cells (Figure 2D). These results suggest that freshly isolated Pmel-1 T cells, particularly *Irf4*$^{-/-}$ Pmel-1 T cells, are not effective in infiltrating B16-F10 tumors.

Next, Thy1.1$^+$ *Irf4*$^{-/-}$ Pmel-1 and Thy1.1$^+$Thy1.2$^+$ WT Pmel-1 T cells were activated *ex vivo* for 24 h by hgp100$_{25–33}$ peptide stimulation. Activated Thy1.1$^+$ *Irf4*$^{-/-}$ Pmel-1 and Thy1.1$^+$Thy1.2$^+$ WT Pmel-1 T cells were then co-injected at a 1:1 ratio into Thy1.2$^+$ WT B6 mice on the same day of B16-F10 implantation (Figure 2A). At two weeks post-cell transfer, Thy1.1$^+$Thy1.2$^+$ WT Pmel-1 T cells were present in spleens and DLNs, and were enriched in tumors. In contrast, Thy1.1$^+$ *Irf4*$^{-/-}$ Pmel-1 T cells were barely detectable in spleens, DLNs and tumors (Figure 2E). Figure 2F shows that the detected Pmel-1 T cells were predominantly WT Pmel-1 T cells, with very low proportions of *Irf4*$^{-/-}$ Pmel-1 T cells. Therefore, the survival of activated Pmel-1 T cells depends on the transcription factor IRF4.

Overexpression of IRF4 enhances tumor infiltration and anti-tumor efficacy of adoptively transferred T cells

To investigate whether overexpressing IRF4 in T cells could enhance their anti-tumor efficacy, we stimulated Thy1.1$^+$ Pmel-1 T cells with hgp100$_{25-33}$ peptide for 24 h and transduced them with either IRF4-GFP or GFP-control vectors. We confirmed successful transduction of over 50% of the Pmel-1 T cells 24 h after transduction, as indicated by GFP expression (Figure 3A). Subsequently, we implanted B16-F10 cells subcutaneously and, on day 3 after implantation, adoptively transferred stimulated Thy1.1$^+$ Pmel-1 T cells (containing 1 x 10^6 GFP$^+$; either IRF4-GFP or GFP-control transduced) to Thy1.2$^+$ B6 mice (Figure 3B). A separate group of mice received no cell transfer. We monitored tumor growth and analyzed the transferred Pmel-1 T cells. Our results showed that adoptive transfer of IRF4-GFP, but not GFP-control transduced Pmel-1 T cells, significantly inhibited B16-F10 melanoma tumor growth in mice (Figure 3C). Therefore, IRF4-engineered adoptive T cell transfer exhibits significant anti-tumor efficacy.

On day 14 after B16-F10 implantation, we observed the presence of transferred Thy1.1$^+$ Pmel-1 T cells in spleens and DLNs from both the IRF4-GFP and GFP-control groups (Figures S1A and S1B). After infiltrating into B16-F10 tumors, these cells retained GFP expression and their frequency of GFP$^+$ cells was similar to that before the cell transfer (Figure S1C). Notably, in the IRF4-GFP group, more than 40% of the CD45$^+$ tumor-infiltrating leukocytes were the transferred Thy1.1$^+$ Pmel-1 T cells, which was significantly higher than the percentage observed in the GFP-control group (Figure 3D). Additionally, tumor-infiltrating Pmel-1 T cells in the IRF4-GFP group expressed significantly higher levels of

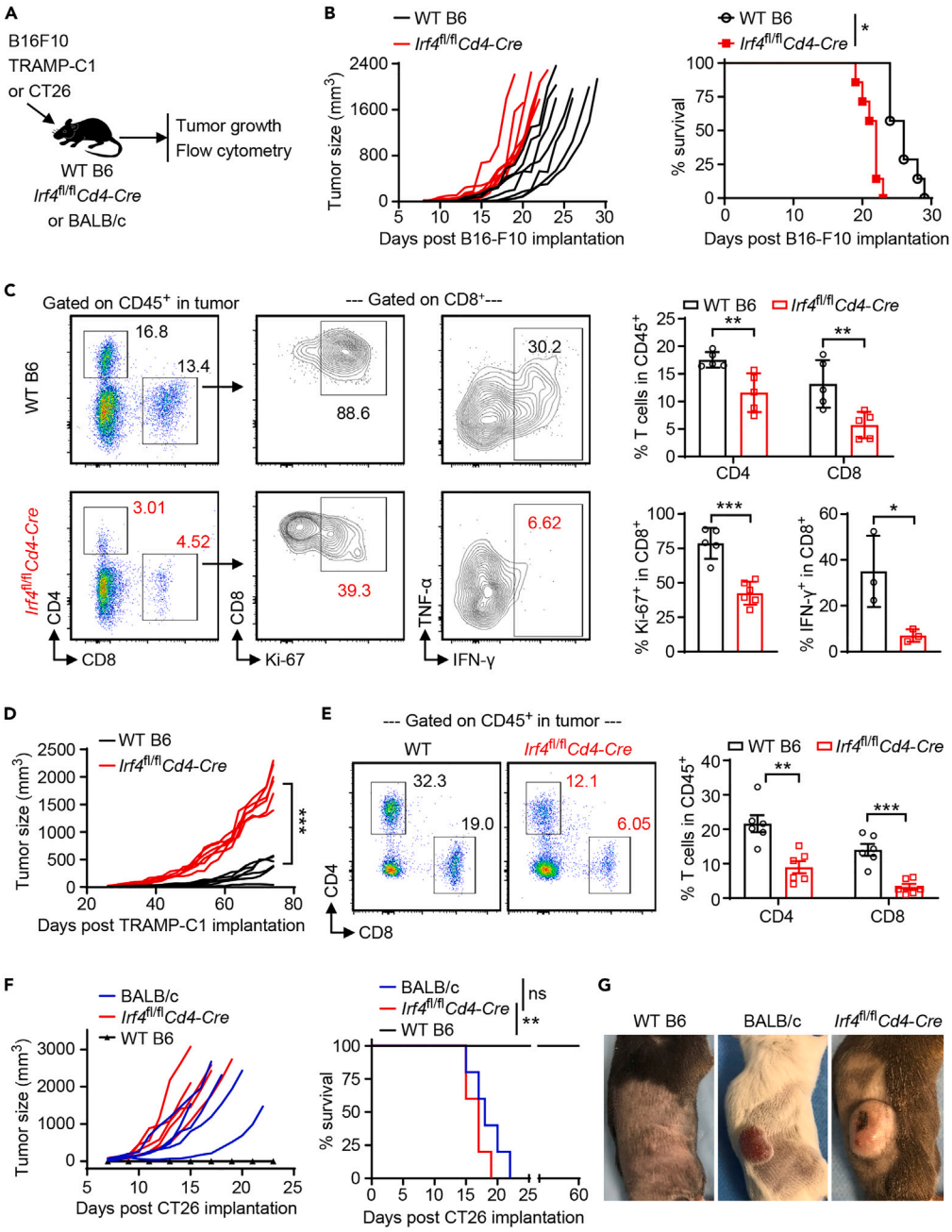

Figure 1. IRF4 is necessary for T cells to exert their anti-tumor immune response

(A) Schematic representation of the experimental design.

(B and C) *Irf4*$^{fl/fl}$*Cd4-Cre* or WT B6 mice were subcutaneously injected with 0.1 x 10^6 B16-F10 cells. (B) Tumor volumes and survival of tumor-bearing *Irf4*$^{fl/fl}$*Cd4-Cre* and WT B6 mice. n = 7/group. (C) Percentages of CD4$^+$ and CD8$^+$ T cells within CD45$^+$ tumor-infiltrating cells (n = 5/group), and percentages of Ki67$^+$ (n = 5/group) and IFN-γ$^+$ (n = 3/group) within CD8$^+$ tumor-infiltrating T cells 20 days post B16-F10 implantation.

(D and E) *Irf4*$^{fl/fl}$*Cd4-Cre* or WT B6 mice were subcutaneously injected with 2 x 10^6 TRAMP-C1 cells. (D) Tumor volumes for *Irf4*$^{fl/fl}$*Cd4-Cre* and WT B6 groups. n = 6/group. (E) % CD4$^+$ and % CD8$^+$ T cells within CD45$^+$ tumor-infiltrating cells (n = 6/group) 74 days post TRAMP-C1 implantation.

(F and G) *Irf4*$^{fl/fl}$*Cd4-Cre*, WT B6, or Balb/c mice were subcutaneously injected with 1 x 10^6 CT26 cells. (F) Tumor volumes and survival of tumor-bearing *Irf4*$^{fl/fl}$*Cd4-Cre*, WT B6, and BALB/c mice. n = 5/group. (G) Representative images showing tumor growth on indicated mouse strains mice at 18 days post CT26 implantation.

Data are presented as mean ± SD (C and E). Statistics applied using the log rank test (B) and an unpaired two-tailed Student's *t* test (C, D [day 74 tumor volumes between 2 groups], and E). *p < 0.05, **p < 0.01, ****p < 0.0001.

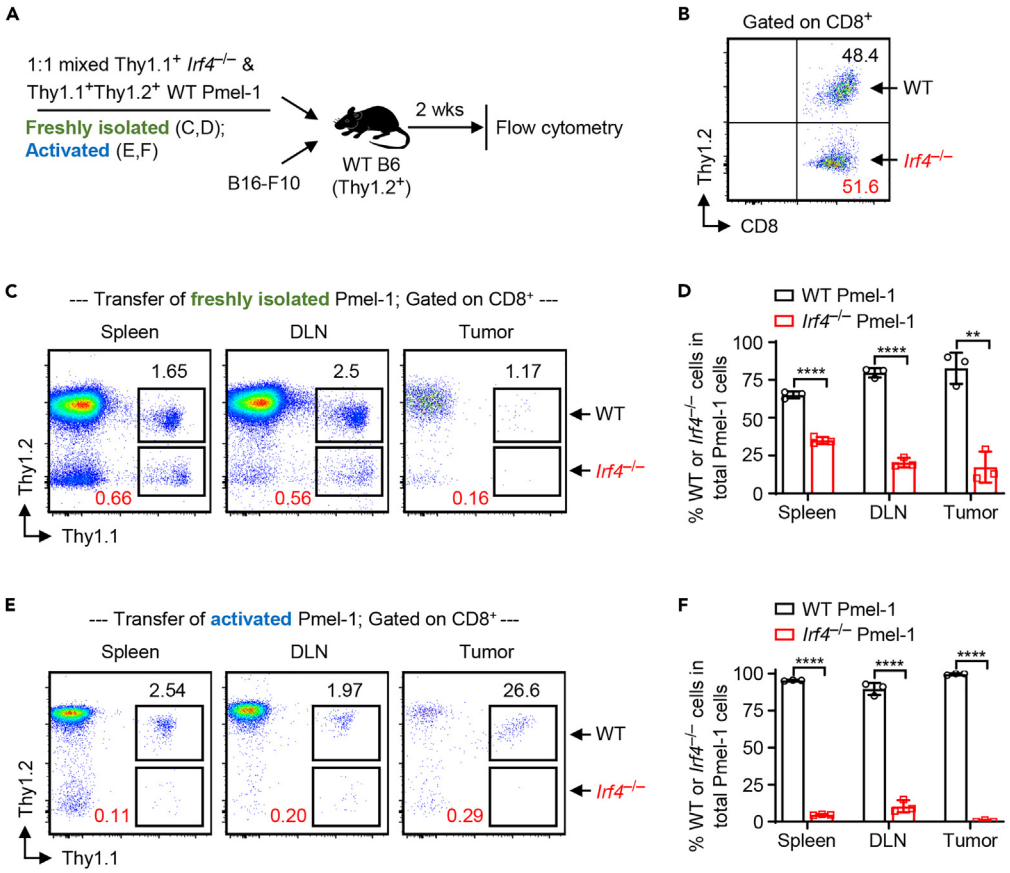

Figure 2. IRF4 is vital for the survival of antitumor CD8$^+$ T cells

(A) Schematic representation of the experimental design.

(B–D) 1 x 10^6 freshly-isolated Thy1.1$^+$ *Irf4*$^{-/-}$ Pmel-1 and 1 x 10^6 freshly isolated Thy1.1$^+$Thy1.2$^+$ WT Pmel-1 T cells were mixed and co-injected into Thy1.2$^+$ WT B6 mice on the same day of B16-F10 implantation. The FACS plot showing representative mixed Pmel-1 T cells before transfer (B). Representative plots display percentages of WT or Pmel-1 T cells within CD8$^+$ T cells (C), and the bar graph shows percentages of WT or *Irf4*$^{-/-}$ Pmel-1 T cells within total Pmel-1 T cells (D) in spleens, DLNs, and tumors at 14 days post-cell transfer.

(E and F) Following a two-day hgp100$_{25\text{-}33}$ peptide stimulation, 1 x 10^6 activated Thy1.1$^+$ *Irf4*$^{-/-}$ Pmel-1 and 1 x 10^6 activated Thy1.1$^+$Thy1.2$^+$ WT Pmel-1 T cells were mixed and co-injected into Thy1.2$^+$ WT B6 mice on the same day of B16-F10 implantation. Representative plots display percentages of WT or Pmel-1 T cells within CD8$^+$ T cells (E), and the bar graph shows percentages of WT or *Irf4*$^{-/-}$ Pmel-1 T cells within total Pmel-1 T cells (F) in spleens, DLNs, and tumors at 14 days post-cell transfer. Data are presented as mean ± SD (D and F; n = 3/group), and the results are representative of two independent experiments. Statistics applied using an unpaired two-tailed Student's *t* test (D and F). **p < 0.01, ****p < 0.0001.

IRF4 and the proliferation marker Ki67 compared to those in the GFP-control group (Figures 3E and S1D. These results were obtained by analyzing total tumor-infiltrating Pmel-1 T cells since the staining method interfered with GFP detection. Furthermore, GFP$^+$ Pmel-1 T cells that infiltrated the tumors in the IRF4-GFP group produced significantly higher levels of pro-inflammatory cytokines IFN-γ and TNF-α than those in the GFP-control group (Figure 3F). Collectively, our data indicate that overexpression of IRF4 in adoptively transferred Pmel-1 T cells promotes their infiltration into tumors and enhances their activity, thereby inhibiting melanoma progression.

IRF4-engineered adoptive T cell therapy combined with PD-L1 blockade inhibits tumor progression

We next evaluated the anti-tumor efficacy of IRF4-engineered adoptive T cell therapy in combination with PD-L1 blockade. On day 3 after implantation of B16-F10 cells, the Thy1.2$^+$ B6 mice were adoptively transferred with activated Thy1.1$^+$ Pmel-1 T cells that contained 1 x 10^6 GFP$^+$ cells, which were transduced with either IRF4-GFP or GFP-control. On days 3, 6, and 9, the mice were intraperitoneally injected with 200 μg anti-PD-L1 mAb (Figure 4A). Additional groups of B16-F10 bearing mice received only anti-PD-L1 mAb treatment or no treatment. We observed a moderate reduction in tumor growth with anti-PD-L1 alone (Figure 4B). However, the adoptive transfer of IRF4-GFP transduced Pmel-1 T cells combined with anti-PD-L1 mAb resulted in significantly more effective inhibition of tumor growth than the adoptive transfer of GFP-control transduced Pmel-1 T cells combined with anti-PD-L1 mAb (Figure 4C). These results indicate that the combination of IRF4-engineered adoptive T cell therapy and PD-L1 blockade exhibits potent antitumor efficacy.

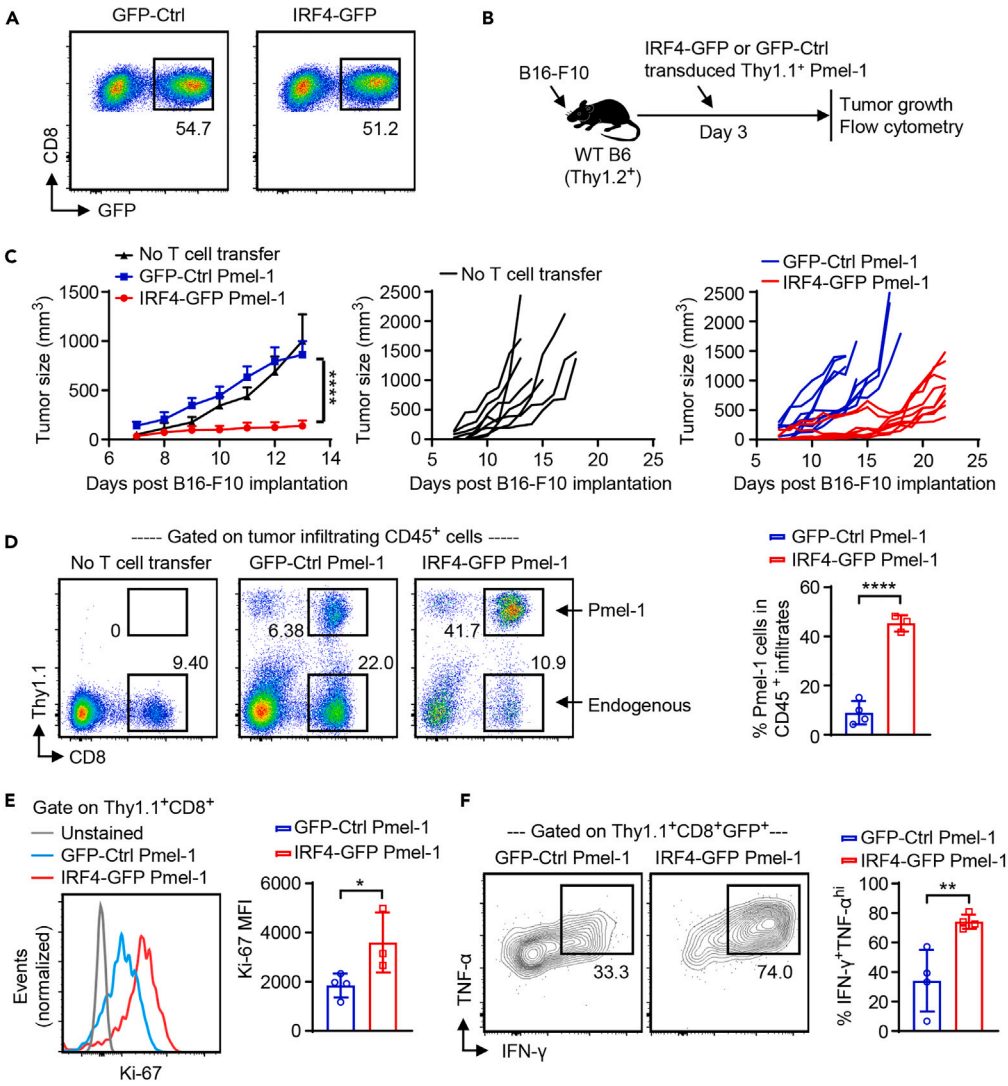

Figure 3. Overexpression of IRF4 enhances tumor infiltration and anti-tumor efficacy of adoptively transferred T cells

(A) Representative FACS plots show percentages of GFP$^+$ cells in cultured Pmel-1 cells before transfer.

(B) Schematic representation of the experimental design. On day 3 post-implantation of 0.5 x 10^6 B16-F10 cells, Thy1.2$^+$ B6 mice were adoptively transferred with cultured Thy1.1$^+$ Pmel-1 cells containing 1 x 10^6 GFP$^+$ Pmel-1 T cells (transduced with either IRF4-GFP or GFP-control [Ctrl]). Mice left without cell transfer serve as a control group.

(C) Mean tumor volumes ±SEM before day 13 (left panel) for IRF4-GFP Pmel-1 (n = 9), GFP-Ctrl Pmel-1 (n = 9), and no T cell transfer (n = 8) groups. At day 13, some mice in the control groups reached endpoint of tumor size. The middle and right panels show the changes in tumor volumes in individual mice.

(D–F) Experiments were repeated to analyze tumor infiltrating cells from each group on day 14 post B16-F10 implantation. (D) Percentages of Pmel-1 T cells within CD45$^+$ tumor infiltrating cells in the IRF4-GFP Pmel-1 and GFP-Ctrl Pmel-1 cell transfer groups. (E) Ki67 expression by tumor infiltrating Pmel-1 cells. (F) Percentages of IFN-γ$^+$TNF-α^{high} cells within tumor infiltrating Pmel-1 cells. Data are presented as mean ± SD (D, E, and F; n = 3–4/group), and the results are representative of two independent experiments. Statistics applied using an unpaired two-tailed Student's *t* test (C [day 13 tumor volumes between the IRF4-GFP Pmel-1 and GFP-Ctrl Pmel-1 groups], D, E, and F). *p < 0.05, **p < 0.01, ****p < 0.0001. See also Figure S1.

Overexpression of IRF4 promotes the functional state transition of adoptively transferred CD8$^+$ T cells in tumors

To better comprehend the enhanced anti-tumor potency of T cells engineered to overexpress IRF4, we utilized scRNA-seq to examine IRF4-transduced anti-tumor T cells that infiltrated tumors. Three days after B16-F10 implantation, Thy1.2$^+$CD45.1$^+$ B6 mice were adoptively transferred with activated Thy1.1$^+$ Pmel-1 T cells that contained 1 x 10^6 GFP$^+$ cells, which were transduced with either IRF4-GFP or GFP-control. Fourteen days after implantation, we isolated Pmel-1 T cells, including both GFP$^+$ and GFP$^-$, from the tumors of the GFP-control group, while only GFP$^+$ Pmel-1 T cells were isolated from the tumors of the IRF4-GFP group to enrich IRF4-transduced cells. We analyzed the isolated tumor-infiltrating Pmel-1 T cells by 10x Genomics scRNA-seq and used Uniform Manifold Approximation and Projection (UMAP) and unsupervised graph-based clustering to partition the tumor-infiltrating Pmel-1 T cells into four clusters based on their transcriptomes (Figures 5A and 5B). Cluster 1, which

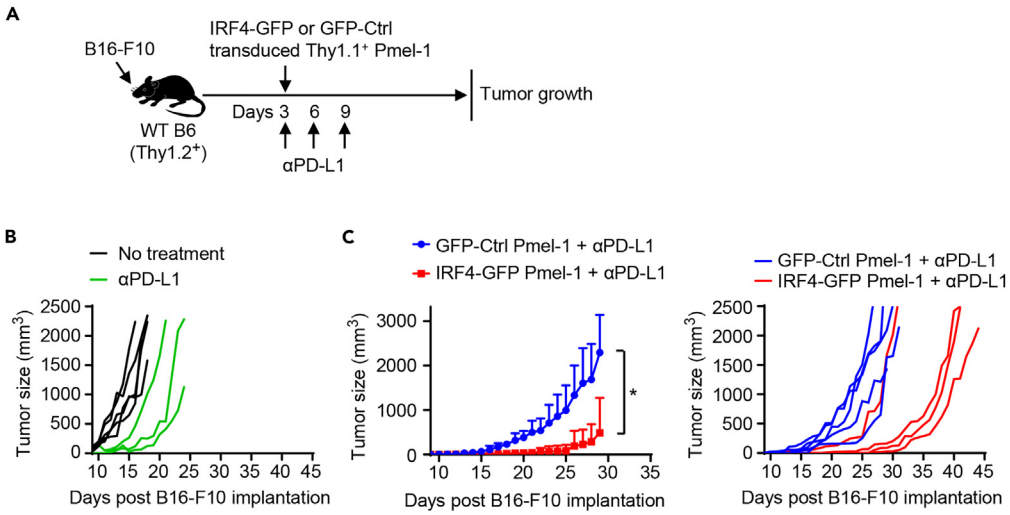

Figure 4. IRF4-engineered adoptive T-cell therapy combined with PD-L1 blockade inhibits tumor progression

(A) Schematic representation of the experimental design. B6 mice were implanted with 0.5 x 10^6 B16-F10 cells and on day 3 were adoptively transferred with cultured Pmel-1 cells containing 1 x 10^6 GFP$^+$ Pmel-1 T cells (transduced with either IRF4-GFP or GFP-ctrl), followed by treatment with 200 μg anti-PD-L1 mAb on days 3, 6, and 9. Control groups included B16-F10–bearing mice receiving anti-PD-L1 mAb alone or no treatment.

(B) Tumor volumes for anti-PD-L1 alone (n = 3) and no treatment (n = 5) groups.

(C) Mean tumor volumes ± SD before day 29 (left panel) for IRF4-GFP Pmel-1 + anti-PD-L1 (n = 4) and GFP-Ctrl Pmel-1 + anti-PD-L1 (n = 5) groups. At day 29, some mice in the GFP-Ctrl Pmel-1 + anti-PD-L1 group reached endpoint of tumor size. The right panel shows the changes in tumor volumes in individual mice. Statistical significance in day 29 tumor volumes between the IRF4-GFP Pmel-1 + anti-PD-L1 and GFP-Ctrl Pmel-1 + anti-PD-L1 groups was determined using an unpaired two-tailed Student's *t* test (C). *p < 0.05.

was enriched for *Tcf7*, *Lef1*, *Bcl2*, *Sell*, and *Il7r*, exhibited a naive/memory-like phenotype and relatively low expression of effector T cell markers and inhibitory receptors. Cluster 2, which highly expressed epigenetic regulators *Ezh2*, *Dnmt1*, *Dnmt3a*, *Hdac1*, and *Hat1*, showed down-regulation of naive/memory-like cell markers and weak expression of effector T cell markers. Clusters 3 and 4, which highly expressed effector T cell markers *Gzmb*, *Prf1*, *Ifng*, and *Tnfrsf9*, had lost a naive/memory-like cell phenotype (Figures 5C and 5D). Clusters C3 and C4 were distinct based on the expression of *Prdm1*, *Gzmk*, and *Havcr2* in C3, and the expression of *Nr4a1* and *Nr4a3* in C4 (Figure S2A). However, the distinct functional roles, as well as the potential implications of these effector cell subsets, remain unclear.

The distribution of tumor-infiltrating Pmel-1 T cells from the GFP-control group was as follows: 47.5% were in the naive/memory-like cluster 1, 27.7% in the epigenetic regulators-enriched cluster 2, and only 24.8% developed into effector T cells (combining clusters 3 and 4). Conversely, among the tumor-infiltrating Pmel-1 T cells from the IRF4-GFP group, only 25.2% and 21.2% were identified in clusters 1 and 2, respectively, while 53.6% had successfully transitioned into effector T cells (combining clusters 3 and 4) (Figure S2B). These results indicate that overexpression of IRF4 promotes the transition of Pmel-1 T cells into effector cell states in tumors.

Cluster C3 is distinguished from cluster C4 based on its expression of *Havcr2*, which encodes the T cell exhaustion marker Tim3. To investigate whether overexpressing IRF4 in Pmel-1 cells could enhance the expression of Tim3 and other inhibitory receptors, we implanted B16-F10 cells into Thy1.2$^+$ B6 mice. Three days later, the mice were adoptively transferred with activated Thy1.1$^+$ Pmel-1 T cells that contained 1 x 10^6 GFP$^+$ cells (transduced with either IRF4-GFP or GFP-control). The GFP$^+$ tumor-infiltrating Pmel-1 T cells were analyzed 14 days after B16-F10 implantation. Notably, compared to the GFP-control group, the GFP$^+$ tumor-infiltrating Pmel-1 T cells from the IRF4-GFP group showed increased frequencies of cells expressing Granzyme B, Tigit, Tim3, and Lag3 (Figures S3A and S3B). Therefore, overexpression of IRF4 in tumor-infiltrating Pmel-1 cells enhances the expression of both granzyme B and several inhibitory receptors.

Adoptive transfer of IRF4-overexpressing T cells invigorates the endogenous CD8$^+$ T cell response in tumors

To investigate the impact of adoptive transfer of IRF4-overexpressing T cells on endogenous anti-tumor immunity, we performed scRNA-seq on Thy1.1$^-$CD45.1$^+$ endogenous immune cells isolated from B16-F10 tumors of either the IRF4-GFP or GFP-control group (Figure 5A), concurrently with Pmel-1 cell isolation. Using UMAP and unsupervised graph-based clustering, we segregated the endogenous tumor-infiltrating immune cells into 10 distinct clusters, including CD4$^+$ T cells, Foxp3$^+$ regulatory T cells, CD8$^+$ T cells, NK cells, dendritic cells, macrophages (two clusters), B cells, Basophils, and a small cluster with unknown cell identity (Figures 6A and S4A).

We utilized UMAP to visualize the endogenous tumor-infiltrating immune cells of the IRF4-GFP and GFP-control groups separately (Figure 6B), followed by an examination of the expression of individual genes. We observed distinct patterns of expression for markers of naive/memory-like T cells (*Tcf7*, *Il7r*, and *Bcl2*) and effector cells (*Gzmb*, *Prf1*, *Ifng*, and *Pdcd1*) within the endogenous CD8$^+$ T cell cluster (Figures 6C and S4B). Importantly, the IRF4-GFP group exhibited an increase in endogenous CD8$^+$ tumor-infiltrating cells that had differentiated into effector T cells (expressing *Gzmb*, *Prf1*, and *Ifng*) compared to the GFP-control group. These findings demonstrate that the adoptive transfer of IRF4-overexpressing

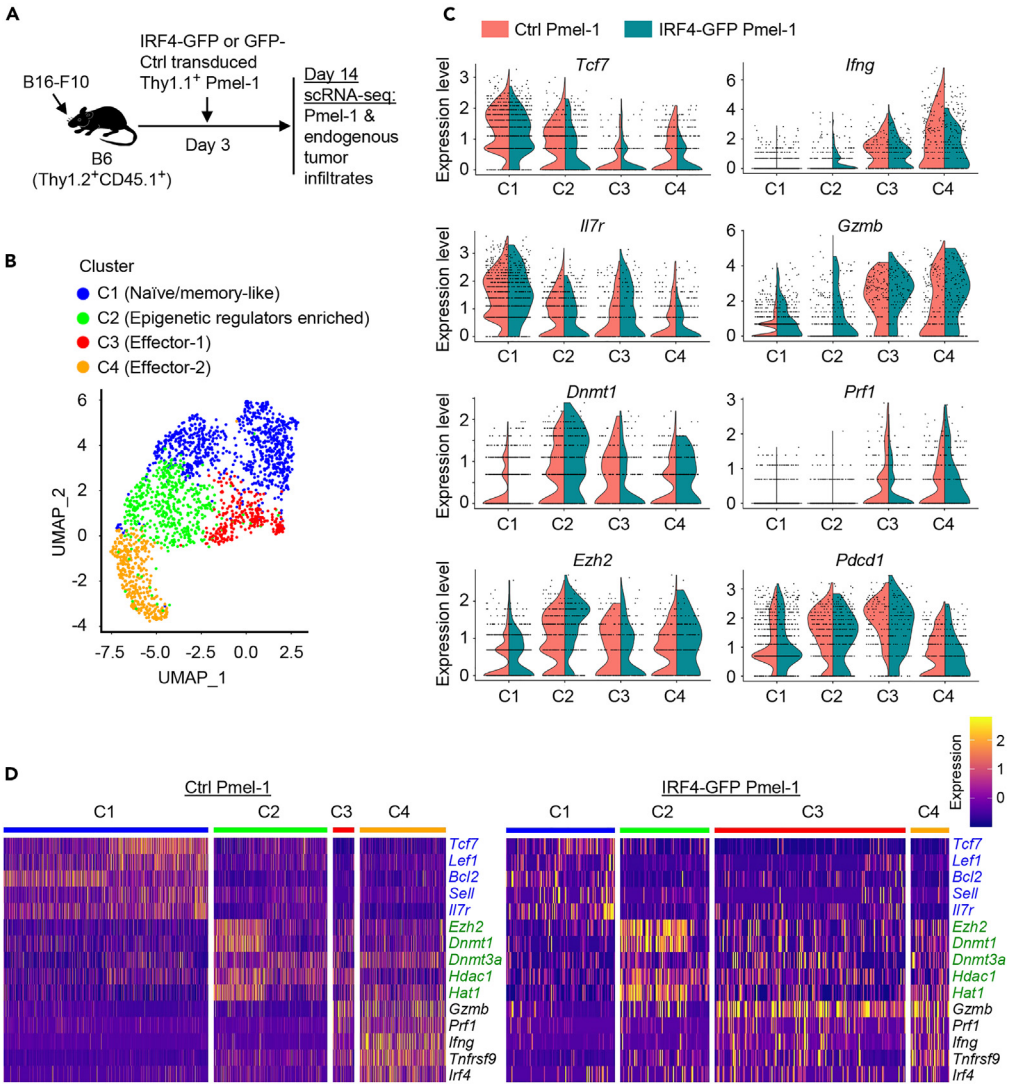

Figure 5. Overexpression of IRF4 promotes the functional state transition of adoptively transferred CD8$^+$ T cells in tumors

(A) Schematic representation of the experimental design. Thy1.2$^+$CD45.1$^+$ B6 mice were implanted with 0.5 x 10^6 B16-F10 cells and on day 3 were adoptively transferred with cultured Thy1.1$^+$ Pmel-1 cells containing 1 x 10^6 GFP$^+$ Pmel-1 T cells (transduced with either IRF4-GFP or GFP-ctrl). On day 14, Ctrl Pmel-1 (including both GFP$^+$ and GFP$^-$) and IRF4-GFP$^+$ Pmel-1 (including GFP$^+$ only) T cells were isolated from the tumors of the GFP-Ctrl group and the IRF4-GFP group, respectively, followed by scRNA-seq analysis.

(B) The UMAP projection of tumor infiltrating Pmel-1 cells, including both Ctrl Pmel-1 and IRF4-GFP$^+$ Pmel-1 cells. Four clusters (C1 to C4) were identified using the Shared Nearest Neighbor (SNN) algorithm with a resolution parameter 0.8. Each dot corresponds to one single cell and is colored according to cell cluster.

(C) Split violin plots show the expression of selected genes in C1-C4 clusters of either Ctrl Pmel-1 or IRF4-GFP$^+$ Pmel-1 cells. The expression levels were normalized by log (raw read count +1) for each gene in the cells of each cluster.

(D) Heatmaps display scaled expression values of selected genes (in rows) in C1-C4 clusters of either Ctrl Pmel-1 or IRF4-GFP$^+$ Pmel-1 cells. The columns correspond to the cells and are grouped by clusters. To explore the relative abundance of gene expression in each cell, *Z* score statistics was used to scale the gene expression counts. For visualization, the extreme z-scores above 3 were truncated to 3 to prevent the impact of outliers. See also Figures S2 and S3.

T cells can enhance the endogenous CD8$^+$ T cell response in tumors. Furthermore, in both groups, endogenous NK cells exhibit expression of *Gzmb* and *Prf1*, while endogenous CD4$^+$ cells display naive/memory-like markers *Tcf7* and *Il7r* (Figures 6C and S4B). The impact of IRF4-GFP Pmel-1 cell transfer on endogenous NK cells, CD4$^+$ T cells, and other immune cells remains an area for future evaluation.

DISCUSSION

The transcriptional programs that regulate T cell infiltration and functional states in tumors have not been adequately studied. In our current study, we found that the transcription factor IRF4 plays a crucial role in regulating anti-tumor T cell immunity. Deletion of IRF4 led to a loss of

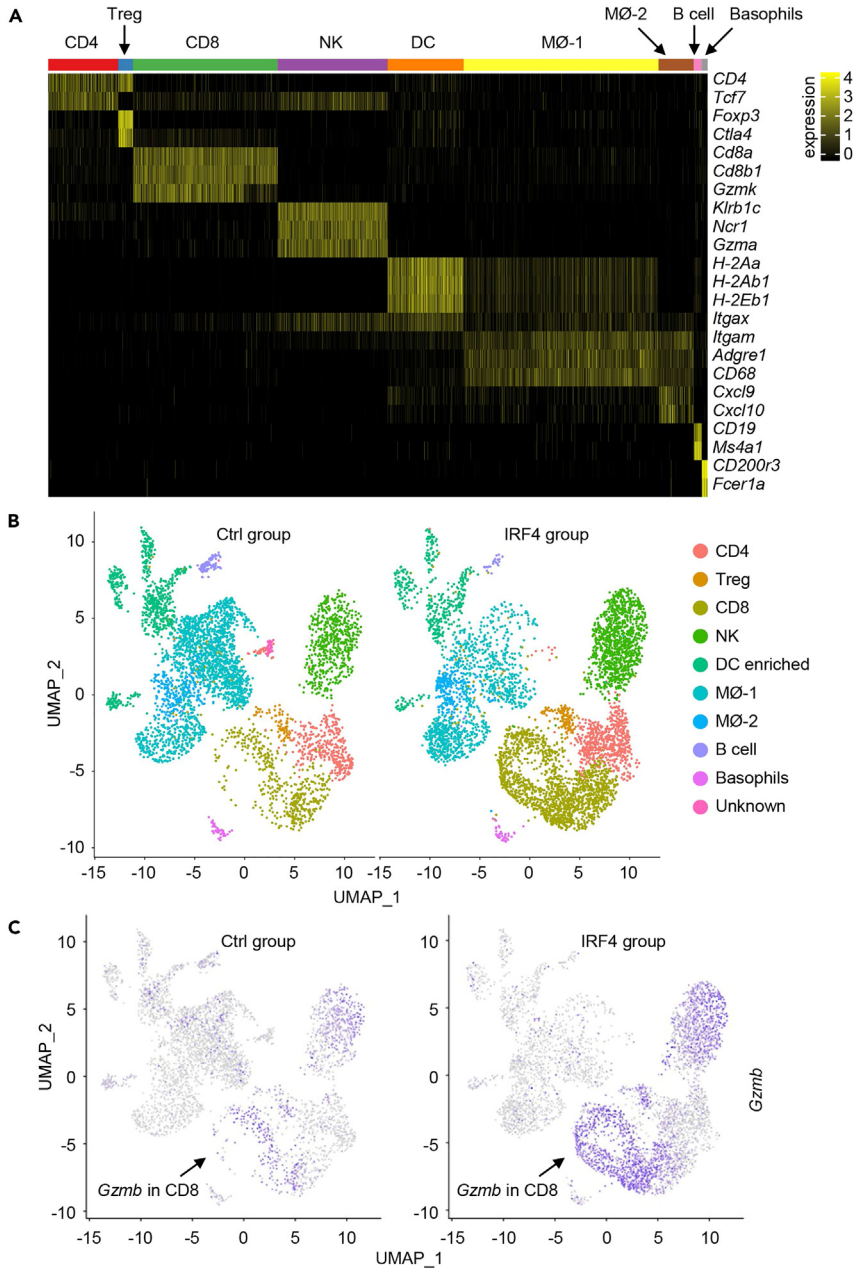

Figure 6. IRF4-engineered adoptive T cell therapy enhances endogenous CD8$^+$ T cell response in tumors

Thy1.1$^-$CD45.1$^+$ endogenous immune cells were isolated from B16-F10 tumors of either the IRF4-GFP or GFP-control group (illustrated in Figure 5A), followed by scRNA-Seq analysis.

(A) Heatmap shows scaled expression values of discriminative gene sets for each cell type, and includes cells from both groups. The columns correspond to the cells and are grouped by clusters representing different cell types.

(B) UMAP plots show cell clusters in either the Ctrl group (transferred with GFP-control Pmel-1 cells) or the IRF4 group (transferred with IRF4-GFP Pmel-1 cells). Ten clusters of endogenous tumor-infiltrating immune cells were identified using the SNN algorithm with a resolution parameter 0.8. Each dot corresponds to a single cell and is colored according to cell cluster.

(C) UMAP plots display the single-cell transcript levels of *Gzmb* in either the Ctrl group or the IRF4 group (gray, not expressed; purple, expressed). See also Figure S4.

T cell immunity against subcutaneous syngeneic and allogeneic tumors. Conversely, in adoptive T cell therapy, overexpressing IRF4 promoted T cell infiltration and facilitated a functional state transition of T cells in tumors, leading to a substantial improvement in their anti-tumor efficacy.

The Pmel-1 adoptive transfer model is frequently used to develop strategies for improving adoptive T cell therapy.[27–29] To achieve anti-tumor efficacy, Pmel-1 cells are typically stimulated/invigorated using various approaches, including sub-lethal irradiation of B16-bearing recipient mice, *in vitro* activation of Pmel-1 cells before cell transfer, antigen-specific vaccination, and administration of IL-2. Adoptive transfer of Pmel-1 cells alone, whether freshly isolated or *in vitro* activated, generally does not inhibit the growth of subcutaneous B16 melanoma.[27–29] Our scRNA-seq analysis explains why Pmel-1 adoptive transfer alone typically fails to prevent tumor growth. Tumor-infiltrating Pmel-1 cells from the GFP-control group were mainly found in the naive/memory-like cluster and the epigenetic regulators-enriched cluster, with only 24.8% of them found in effector T cell clusters, which corresponds to their limited anti-tumor effects. However, in contrast to the ineffectiveness of control Pmel-1 cells, adoptive transfer of IRF4-overexpressing Pmel-1 cells (even when used alone) demonstrated significant anti-tumor efficacy. As a result of improved anti-tumor activity, 53.6% of tumor-infiltrating Pmel-1 cells from the IRF4-overexpressing group had transitioned into effector T cells successfully. These findings emphasize the importance of IRF4-engineering for adoptive T cell therapy.

T cell exhaustion refers to a dysfunctional state of T cells, marked by loss of effector functions and high expression of inhibitory receptors PD-1, TIM-3, LAG-3, and TIGIT.[30,31] The NFAT-NR4A and NFAT-TOX axes drive T cell exhaustion by promoting the expression of multiple inhibitory receptors.[11,32–34] Here, we noticed that the cluster C3 of tumor-infiltrating Pmel-1 cells expressed *Havcr2* (encoding TIM3), and cluster C4 expressed *Nr4a1* and *Nr4a3*. However, C3 and C4 exhibited high expression of *Ifng*, *Gzmb*, and *Prf1*, indicating that these cells were still effector T cells. The ineffectiveness of GFP-control Pmel-1 cells was associated with insufficient development of C3 and C4 effector T cells, rather than being exhausted.

In previous studies, we demonstrated that the ablation of IRF4 in T cells induces immune tolerance toward transplanted allografts.[25,26] This occurs through the gradual development of allogeneic $CD4^+$ T cell dysfunction. IRF4 represses Helios and PD-1 expression in activated WT $CD4^+$ T cells. In the absence of IRF4, Helios is expressed at higher levels and binds to PD-1 *cis*-regulatory elements to enhance PD-1 expression in $CD4^+$ T cells.[26] Interestingly, Man et al.[35] used $Irf4^{+/-}$ P14 T cells to investigate the role of IRF4 in $CD8^+$ T cell anti-viral immunity. They found that compared to WT P14 cells, $Irf4^{+/-}$ P14 cells exhibit less exhaustion in response to chronic LCMV infection, displaying lower expression of inhibitory receptors such as PD-1 and TIM-3 and higher expression of naive/memory markers such as TCF1, CD62L, and IL-7R.[35] These findings suggest that IRF4 plays distinct roles in $CD4^+$ T cell dysfunction and $CD8^+$ T cell exhaustion.[36] The chronic LCMV infection model is well-suited for investigating $CD8^+$ T cell exhaustion,[37] whereas in the Pmel-1 adoptive therapy model, control WT Pmel-1 $CD8^+$ T cells were not sufficiently stimulated, instead of being exhausted. In this model, engineered IRF4 overexpression revitalized Pmel-1 cells in tumors, resulting in a significant improvement in anti-tumor efficacy. However, IRF4 plays a dual role in $CD8^+$ T cell activity and exhaustion. Overexpressing IRF4 in tumor-infiltrating Pmel-1 cells notably increases the expression of multiple inhibitory receptors. The inability of transferred IRF4-GFP Pmel-1 cells to eradicate B16F10 tumors suggests that these cells might eventually reach a state of exhaustion.

In summary, the importance of transcription factors in determining T cell functional states suggests that transcription factor engineering could be a promising approach for enhancing adoptive T cell immunotherapy. In this study, we demonstrate that IRF4 is a crucial cell-intrinsic regulator of T cell infiltration and function in tumors, and importantly, IRF4 engineering leads to a significant improvement in the efficacy of adoptive T cell therapy. Further research is needed to assess the applicability of our findings to human T cells.

Limitations of the study

Our research underscores the pivotal role of IRF4 in antitumor immunity; however, the molecular mechanisms underlying its function remain unclear. For instance, IRF4 is mainly expressed in T cells following antigen stimulation, and it does not influence the survival of naive T cells. This raises the question: why do activated anti-tumor $CD8^+$ T cells rely on IRF4 for survival? Furthermore, it is imperative to understand how physiological levels of IRF4, compared to its overexpression, differentially influence the expression of genes encoding key effector molecules and inhibitory receptors. Follow-up studies are crucial and should focus on identifying the genes that IRF4 regulates in anti-tumor T cells, especially those tied to T cell survival, effector differentiation, and exhaustion.

STAR★METHODS

Detailed methods are provided in the online version of this paper and include the following:

- KEY RESOURCES TABLE
- RESOURCE AVAILABILITY
  - Lead contact
  - Materials availability
  - Data and code availability
- EXPERIMENTAL MODEL AND STUDY PARTICIPANT DETAILS
  - Mice
  - Cell lines
- METHOD DETAILS
  - *In vivo* tumor growth
  - Tumor growth in $Irf4^{fl/fl}Cd4\text{-}Cre$ *vs.* WT mice
  - Tumor processing for TIL analysis
  - Flow cytometry analysis

- Tracking *Irf4*$^{-/-}$ *vs.* WT Pmel-1 cells *in vivo*
- Overexpressing IRF4 via retroviral transduction
- ACT using IRF4-transduced Pmel-1 cells
- ScRNA-seq of Pmel-1 and endogenous TILs
- ACT using Pmel-1 cells plus PD-L1 blockade

- QUANTIFICATION AND STATISTICAL ANALYSIS

SUPPLEMENTAL INFORMATION

Supplemental information can be found online at https://doi.org/10.1016/j.isci.2023.108087.

ACKNOWLEDGMENTS

The authors would like to thank the Single Cell Genomics Core at Baylor College of Medicine (partially supported by NIH shared instrument grants [S10OD023469, S10OD025240], P30EY002520 and CPRIT grant RP200504) and the Houston Methodist Flow Cytometry Core Facility for excellent services. This study was supported by internal fund from Houston Methodist Research Institute (to W.C.).

AUTHOR CONTRIBUTIONS

H.Y., X.X., X.C.L., and W.C. conceived and designed the project. H.Y., H.Z., X.X., X.Z., J.F., D.Z., A.Y., and T.J. performed experiments. Y.D. and Z.Z. performed computational analyses of scRNA-seq data. H.Y., Y.D., D.Z., and W.C. analyzed data. X.X., X.Z., D.Z., X.C.L., and Z.Z. performed critical reviews of the manuscript. H.Y., Y.D., and W.C. wrote the manuscript.

DECLARATION OF INTERESTS

The authors declare no competing interests. We have a patent application related to this work. Publication of WO2019168914A1.

Received: March 30, 2023
Revised: May 22, 2023
Accepted: September 25, 2023
Published: September 28, 2023

REFERENCES

1. Sharma, P., and Allison, J.P. (2020). Dissecting the mechanisms of immune checkpoint therapy. Nat. Rev. Immunol. *20*, 75–76. https://doi.org/10.1038/s41577-020-0275-8.
2. Weber, E.W., Maus, M.V., and Mackall, C.L. (2020). The Emerging Landscape of Immune Cell Therapies. Cell *181*, 46–62. https://doi.org/10.1016/j.cell.2020.03.001.
3. Kurtulus, S., Madi, A., Escobar, G., Klapholz, M., Nyman, J., Christian, E., Pawlak, M., Dionne, D., Xia, J., Rozenblatt-Rosen, O., et al. (2019). Checkpoint Blockade Immunotherapy Induces Dynamic Changes in PD-1(-)CD8(+) Tumor-Infiltrating T Cells. Immunity *50*, 181–194.e6. https://doi.org/10.1016/j.immuni.2018.11.014.
4. Siddiqui, I., Schaeuble, K., Chennupati, V., Fuertes Marraco, S.A., Calderon-Copete, S., Pais Ferreira, D., Carmona, S.J., Scarpellino, L., Gfeller, D., Pradervand, S., et al. (2019). Intratumoral Tcf1(+)PD-1(+)CD8(+) T Cells with Stem-like Properties Promote Tumor Control in Response to Vaccination and Checkpoint Blockade Immunotherapy. Immunity *50*, 195–211.e10. https://doi.org/10.1016/j.immuni.2018.12.021.
5. Brunner-Weinzierl, M.C., and Rudd, C.E. (2018). CTLA-4 and PD-1 Control of T-Cell Motility and Migration: Implications for Tumor Immunotherapy. Front. Immunol. *9*, 2737. https://doi.org/10.3389/fimmu.2018.02737.
6. Smith-Garvin, J.E., Koretzky, G.A., and Jordan, M.S. (2009). T cell activation. Annu. Rev. Immunol. *27*, 591–619. https://doi.org/10.1146/annurev.immunol.021908.132706.
7. Barnes, S.E., Wang, Y., Chen, L., Molinero, L.L., Gajewski, T.F., Evaristo, C., and Alegre, M.L. (2015). T cell-NF-kappaB activation is required for tumor control *in vivo*. J. Immunother. Cancer *3*, 1. https://doi.org/10.1186/s40425-014-0045-x.
8. Lynn, R.C., Weber, E.W., Sotillo, E., Gennert, D., Xu, P., Good, Z., Anbunathan, H., Lattin, J., Jones, R., Tieu, V., et al. (2019). c-Jun overexpression in CAR T cells induces exhaustion resistance. Nature *576*, 293–300. https://doi.org/10.1038/s41586-019-1805-z.
9. Seo, H., González-Avalos, E., Zhang, W., Ramchandani, P., Yang, C., Lio, C.W.J., Rao, A., and Hogan, P.G. (2021). BATF and IRF4 cooperate to counter exhaustion in tumor-infiltrating CAR T cells. Nat. Immunol. *22*, 983–995. https://doi.org/10.1038/s41590-021-00964-8.
10. Gonzalez, N.M., Zou, D., Gu, A., and Chen, W. (2021). Schrodinger's T Cells: Molecular Insights Into Stemness and Exhaustion. Front. Immunol. *12*, 725618. https://doi.org/10.3389/fimmu.2021.725618.
11. Chen, J., López-Moyado, I.F., Seo, H., Lio, C.W.J., Hempleman, L.J., Sekiya, T., Yoshimura, A., Scott-Browne, J.P., and Rao, A. (2019). NR4A transcription factors limit CAR T cell function in solid tumours. Nature *567*, 530–534. https://doi.org/10.1038/s41586-019-0985-x.
12. Huber, M., and Lohoff, M. (2014). IRF4 at the crossroads of effector T-cell fate decision. Eur. J. Immunol. *44*, 1886–1895. https://doi.org/10.1002/eji.201344279.
13. Ochiai, K., Maienschein-Cline, M., Simonetti, G., Chen, J., Rosenthal, R., Brink, R., Chong, A.S., Klein, U., Dinner, A.R., Singh, H., and Sciammas, R. (2013). Transcriptional regulation of germinal center B and plasma cell fates by dynamical control of IRF4. Immunity *38*, 918–929. https://doi.org/10.1016/j.immuni.2013.04.009.
14. Vander Lugt, B., Khan, A.A., Hackney, J.A., Agrawal, S., Lesch, J., Zhou, M., Lee, W.P., Park, S., Xu, M., DeVoss, J., et al. (2014). Transcriptional programming of dendritic cells for enhanced MHC class II antigen presentation. Nat. Immunol. *15*, 161–167. https://doi.org/10.1038/ni.2795.
15. Man, K., Miasari, M., Shi, W., Xin, A., Henstridge, D.C., Preston, S., Pellegrini, M., Belz, G.T., Smyth, G.K., Febbraio, M.A., et al. (2013). The transcription factor IRF4 is essential for TCR affinity-mediated metabolic programming and clonal expansion of T cells. Nat. Immunol. *14*, 1155–1165. https://doi.org/10.1038/ni.2710.
16. Zheng, Y., Chaudhry, A., Kas, A., deRoos, P., Kim, J.M., Chu, T.T., Corcoran, L., Treuting, P., Klein, U., and Rudensky, A.Y. (2009). Regulatory T-cell suppressor program co-opts transcription factor IRF4 to control T(H)2 responses. Nature *458*, 351–356. https://doi.org/10.1038/nature07674.
17. Yao, S., Buzo, B.F., Pham, D., Jiang, L., Taparowsky, E.J., Kaplan, M.H., and Sun, J. (2013). Interferon regulatory factor 4 sustains CD8(+) T cell expansion and effector differentiation. Immunity *39*, 833–845. https://doi.org/10.1016/j.immuni.2013.10.007.

18. Staudt, V., Bothur, E., Klein, M., Lingnau, K., Reuter, S., Grebe, N., Gerlitzki, B., Hoffmann, M., Ulges, A., Taube, C., et al. (2010). Interferon-regulatory factor 4 is essential for the developmental program of T helper 9 cells. Immunity *33*, 192–202. https://doi.org/10.1016/j.immuni.2010.07.014.
19. Huber, M., Brüstle, A., Reinhard, K., Guralnik, A., Walter, G., Mahiny, A., von Löw, E., and Lohoff, M. (2008). IRF4 is essential for IL-21-mediated induction, amplification, and stabilization of the Th17 phenotype. Proc. Natl. Acad. Sci. USA *105*, 20846–20851. https://doi.org/10.1073/pnas.0809077106.
20. Cretney, E., Xin, A., Shi, W., Minnich, M., Masson, F., Miasari, M., Belz, G.T., Smyth, G.K., Busslinger, M., Nutt, S.L., and Kallies, A. (2011). The transcription factors Blimp-1 and IRF4 jointly control the differentiation and function of effector regulatory T cells. Nat. Immunol. *12*, 304–311. https://doi.org/10.1038/ni.2006.
21. Brüstle, A., Heink, S., Huber, M., Rosenplänter, C., Stadelmann, C., Yu, P., Arpaia, E., Mak, T.W., Kamradt, T., and Lohoff, M. (2007). The development of inflammatory T(H)-17 cells requires interferon-regulatory factor 4. Nat. Immunol. *8*, 958–966. https://doi.org/10.1038/ni1500.
22. Bollig, N., Brüstle, A., Kellner, K., Ackermann, W., Abass, E., Raifer, H., Camara, B., Brendel, C., Giel, G., Bothur, E., et al. (2012). Transcription factor IRF4 determines germinal center formation through follicular T-helper cell differentiation. Proc. Natl. Acad. Sci. USA *109*, 8664–8669. https://doi.org/10.1073/pnas.1205834109.
23. Mittrücker, H.W., Matsuyama, T., Grossman, A., Kündig, T.M., Potter, J., Shahinian, A., Wakeham, A., Patterson, B., Ohashi, P.S., and Mak, T.W. (1997). Requirement for the transcription factor LSIRF/IRF4 for mature B and T lymphocyte function. Science *275*, 540–543. https://doi.org/10.1126/science.275.5299.540.
24. Grusdat, M., McIlwain, D.R., Xu, H.C., Pozdeev, V.I., Knievel, J., Crome, S.Q., Robert-Tissot, C., Dress, R.J., Pandyra, A.A., Speiser, D.E., et al. (2014). IRF4 and BATF are critical for CD8(+) T-cell function following infection with LCMV. Cell Death Differ. *21*, 1050–1060. https://doi.org/10.1038/cdd.2014.19.
25. Zhang, H., Wu, J., Zou, D., Xiao, X., Yan, H., Li, X.C., and Chen, W. (2019). Ablation of interferon regulatory factor 4 in T cells induces "memory" of transplant tolerance that is irreversible by immune checkpoint blockade. Am. J. Transplant. *19*, 884–893. https://doi.org/10.1111/ajt.15196.
26. Wu, J., Zhang, H., Shi, X., Xiao, X., Fan, Y., Minze, L.J., Wang, J., Ghobrial, R.M., Xia, J., Sciammas, R., et al. (2017). Ablation of Transcription Factor IRF4 Promotes Transplant Acceptance by Driving Allogenic CD4(+) T Cell Dysfunction. Immunity *47*, 1114–1128.e6. https://doi.org/10.1016/j.immuni.2017.11.003.
27. Vo, D.D., Prins, R.M., Begley, J.L., Donahue, T.R., Morris, L.F., Bruhn, K.W., de la Rocha, P., Yang, M.Y., Mok, S., Garban, H.J., et al. (2009). Enhanced antitumor activity induced by adoptive T-cell transfer and adjunctive use of the histone deacetylase inhibitor LAQ824. Cancer Res. *69*, 8693–8699. https://doi.org/10.1158/0008-5472.CAN-09-1456.
28. Hwang, L.N., Yu, Z., Palmer, D.C., and Restifo, N.P. (2006). The *in vivo* expansion rate of properly stimulated transferred CD8+ T cells exceeds that of an aggressively growing mouse tumor. Cancer Res. *66*, 1132–1138. https://doi.org/10.1158/0008-5472.CAN-05-1679.
29. Overwijk, W.W., Theoret, M.R., Finkelstein, S.E., Surman, D.R., de Jong, L.A., Vyth-Dreese, F.A., Dellemijn, T.A., Antony, P.A., Spiess, P.J., Palmer, D.C., et al. (2003). Tumor regression and autoimmunity after reversal of a functionally tolerant state of self-reactive CD8+ T cells. J. Exp. Med. *198*, 569–580. https://doi.org/10.1084/jem.20030590.
30. McLane, L.M., Abdel-Hakeem, M.S., and Wherry, E.J. (2019). CD8 T Cell Exhaustion During Chronic Viral Infection and Cancer. Annu. Rev. Immunol. *37*, 457–495. https://doi.org/10.1146/annurev-immunol-041015-055318.
31. Blank, C.U., Haining, W.N., Held, W., Hogan, P.G., Kallies, A., Lugli, E., Lynn, R.C., Philip, M., Rao, A., Restifo, N.P., et al. (2019). Defining 'T cell exhaustion'. Nat. Rev. Immunol. *19*, 665–674. https://doi.org/10.1038/s41577-019-0221-9.
32. Liu, X., Wang, Y., Lu, H., Li, J., Yan, X., Xiao, M., Hao, J., Alekseev, A., Khong, H., Chen, T., et al. (2019). Genome-wide analysis identifies NR4A1 as a key mediator of T cell dysfunction. Nature *567*, 525–529. https://doi.org/10.1038/s41586-019-0979-8.
33. Khan, O., Giles, J.R., McDonald, S., Manne, S., Ngiow, S.F., Patel, K.P., Werner, M.T., Huang, A.C., Alexander, K.A., Wu, J.E., et al. (2019). TOX transcriptionally and epigenetically programs CD8(+) T cell exhaustion. Nature *571*, 211–218. https://doi.org/10.1038/s41586-019-1325-x.
34. Scott, A.C., Dündar, F., Zumbo, P., Chandran, S.S., Klebanoff, C.A., Shakiba, M., Trivedi, P., Menocal, L., Appleby, H., Camara, S., et al. (2019). TOX is a critical regulator of tumour-specific T cell differentiation. Nature *571*, 270–274. https://doi.org/10.1038/s41586-019-1324-y.
35. Man, K., Gabriel, S.S., Liao, Y., Gloury, R., Preston, S., Henstridge, D.C., Pellegrini, M., Zehn, D., Berberich-Siebelt, F., Febbraio, M.A., et al. (2017). Transcription Factor IRF4 Promotes CD8(+) T Cell Exhaustion and Limits the Development of Memory-like T Cells during Chronic Infection. Immunity *47*, 1129–1141.e5. https://doi.org/10.1016/j.immuni.2017.11.021.
36. Chennupati, V., and Held, W. (2017). Feeling Exhausted? Tuning Irf4 Energizes Dysfunctional T Cells. Immunity *47*, 1009–1011. https://doi.org/10.1016/j.immuni.2017.11.028.
37. Wherry, E.J., Ha, S.J., Kaech, S.M., Haining, W.N., Sarkar, S., Kalia, V., Subramaniam, S., Blattman, J.N., Barber, D.L., and Ahmed, R. (2007). Molecular signature of CD8+ T cell exhaustion during chronic viral infection. Immunity *27*, 670–684. https://doi.org/10.1016/j.immuni.2007.09.006.
38. Stuart, T., Butler, A., Hoffman, P., Hafemeister, C., Papalexi, E., Mauck, W.M., 3rd, Hao, Y., Stoeckius, M., Smibert, P., and Satija, R. (2019). Comprehensive Integration of Single-Cell Data. Cell *177*, 1888–1902.e21. https://doi.org/10.1016/j.cell.2019.05.031.
39. Dobin, A., Davis, C.A., Schlesinger, F., Drenkow, J., Zaleski, C., Jha, S., Batut, P., Chaisson, M., and Gingeras, T.R. (2013). STAR: ultrafast universal RNA-seq aligner. Bioinformatics *29*, 15–21. https://doi.org/10.1093/bioinformatics/bts635.

STAR★METHODS

KEY RESOURCES TABLE

REAGENT or RESOURCE	SOURCE	IDENTIFIER
Antibodies		
Anti-CD45 (clone 30-F11)	BioLegend	Cat#103130; RRID: AB_893339
Anti-CD45.1 (clone A20)	BioLegend	Cat#110726; RRID: AB_893345
Anti-CD4 (clone GK1.5)	BioLegend	Cat#100414; RRID: AB_312699
Anti-CD8 (clone 53-6.7)	BioLegend	Cat#100725; RRID: AB_493425
Anti-IFNγ (clone XMG1.2)	BioLegend	Cat#505810; RRID: AB_315404
Anti-TNFα (clone MP6-XT22)	BioLegend	Cat#506306; RRID: AB_315427
Anti-Granzyme B (clone QA16A02)	BioLegend	Cat#372204; RRID: AB_2687028
Anti-Tim3 (clone RMT3-23)	BioLegend	Cat#119704; RRID: AB_345378
Anti-PD-1 (clone 29F.1A12)	BioLegend	Cat#135206; RRID: AB_1877231
Anti-Lag3 (clone C9B7W)	BioLegend	Cat#125242; RRID: AB_2860660
Anti-Tigit (clone 1G9)	BioLegend	Cat#142106; RRID: AB_10962572
Anti-Ki-67 (clone SolA15)	Thermo Fisher	Cat#25-5698-82; RRID:AB_11220070
Anti-Thy1.1 (clone OX-7)	BioLegend	Cat#202522; RRID: AB_1595477
Anti-Thy1.2 (clone 53-2.1)	BioLegend	Cat#140310; RRID: AB_10643586
Anti-IRF4 (polyclonal M-17)	Santa Cruz	Cat#sc-6059; RRID: AB_2127145
Donkey anti-Goat IgG, Alexa Fluor 647	Thermo Fisher	Cat#A-21447; RRID: AB_2535864
*InVivo*MAb anti-PD-L1 (clone 10F.9G2)	BioXcell	Cat#BE0101; RRID: AB_10949073
Bacterial and virus strains		
pMYs-IRES-GFP Retroviral Vector	Cell Biolabs	Cat#RTV-021
Plat-E Retroviral Packaging Cell Line	Cell Biolabs	Cat#RV-101
Chemicals, peptides, and recombinant proteins		
$hgp100_{25\text{-}33}$ peptide	GenScript	Cat#RP20344
Murine IL-2	PeproTech	Cat#212-12
Phorbol 12-myristate 13-acetate	Sigma-Aldrich	Cat#P8139; CAS:16561-29-8
Ionomycin	Sigma-Aldrich	Cat#I3909; CAS:56092-82-1
Critical commercial assays		
Zombie Aqua™ Fixable Viability Kit	BioLegend	Cat#423102
Foxp3/Transcription Factor Staining Set	Thermo Fisher	Cat#00-5523-00
BD Cytofix/Cytoperm™ with GolgiStop	BD Biosciences	Cat#554715
Chromium Next GEM Single Cell 3′ Reagent Kits v3	10x Genomics	Cat#PN-1000269
Deposited data		
scRNA-seq data	This paper	GEO: GSE227699
Experimental models: Cell lines		
Cell line: B16-F10	American Type Culture Collection	Cat#CRL-6475
Cell line: TRAMP-C1	American Type Culture Collection	Cat#CRL-2730
Cell line: CT26.WT	American Type Culture Collection	Cat#CRL-2638
Experimental models: Organisms/strains		
Mouse: C57BL/6	Jackson Lab	JAX: 000664

(*Continued on next page*)

Continued

REAGENT or RESOURCE	SOURCE	IDENTIFIER
Mouse: BALB/c	Jackson Lab	JAX: 000651
Mouse: CD4-Cre	Jackson Lab	JAX: 022071
Mouse: *Irf4*(fl/fl): B6.129S1-Irf4tm1Rdf/J	Jackson Lab	JAX: 009380
Mouse: B6.SJL CD45.1	Jackson Lab	JAX: 002014
Mouse: Pmel-1: B6.Cg-Thy1a/Cy Tg(TcraTcrb) 8Rest/J	Jackson Lab	JAX: 005023
Mouse: *Irf4*$^{-/-}$: B6.129P2-Irf4tm1Mak/J	Jackson Lab	JAX: 031834
Recombinant DNA		
Plasmid: IRF4-GFP	Wu et al. (2017)[26]	N/A
Software and algorithms		
Cell Ranger v3.0.2	10x Genomics	https://www.10xgenomics.com/
Seurat v3.0.1	Stuart et al. (2019)[38]	https://satijalab.org/seurat/
R v3.6.0	R Development Core Team (2008)	https://www.r-project.org/
FlowJo v10	Tree Star Inc	https://www.flowjo.com/
Prism version 8.0	GraphPad Software	http://www.graphpad.com/scientific-software/prism/

RESOURCE AVAILABILITY

Lead contact

Further information and request for resources and reagents should be directed to and will be fulfilled by the Lead Contact, Wenhao Chen (wchen@houstonmethodist.org).

Materials availability

This study did not generate new unique reagents.

Data and code availability

- Single-cell RNA-seq data have been deposited at GEO and are publicly available as of the date of publication. Accession number is listed in the key resources table.
- This paper does not report original code.
- Any additional information required to reanalyze the data reported in this paper is available from the lead contact upon request.

EXPERIMENTAL MODEL AND STUDY PARTICIPANT DETAILS

Mice

Mice used in this study were obtained from The Jackson Laboratory (Bar Harbor, MA) and included *Cd4-Cre*, *Irf4*$^{flox/flox}$, *Irf4*$^{-/-}$, Pmel-1 TCR-transgenic, B6.SJL CD45.1 congenic, BALB/c, and C57BL/6 (B6) strains. To generate *Irf4*$^{fl/fl}$*Cd4-Cre* mice, *Irf4*$^{flox/flox}$ mice were crossed with *Cd4-Cre* mice. Thy1.1^{+} Pmel-1 mice were crossed with *Irf4*$^{-/-}$ mice to generate Thy1.1^{+} *Irf4*$^{-/-}$ Pmel-1 mice. Thy1.1^{+}Thy1.2^{+} Pmel-1 mice were generated by crossing Thy1.2^{+} WT B6 mice with Thy1.1^{+} Pmel-1 mice. Tumor implantation experiments were conducted using male and female mice that were 8 to 10 weeks old. All mice were housed in a specific pathogen-free facility at Houston Methodist Research Institute in Houston, Texas, and all animal experiments were approved by the Houston Methodist Animal Care Committee in accordance with institutional animal care and use guidelines.

Cell lines

The B16-F10, TRAMP-C1, and CT26.WT (CT26) cell lines were obtained from the American Type Culture Collection (ATCC, Manassas, VA). All cell lines were tested negative for mycoplasma and other pathogens with IDEXX BioAnalytics (Columbia, MO). B16-F10 cells were cultured in DMEM supplemented with 10% heat-inactivated fetal bovine serum (FBS) and 1% penicillin-streptomycin. TRAMP-C1 cells were cultured in DMEM supplemented with 5% heat-inactivated FBS, 5% Nu-Serum™ IV Growth Medium Supplement, 5 μg/mL bovine insulin, 10 nM dehydroisoandrosterone, and 1% penicillin-streptomycin. CT26 cells were cultured in RPMI-1640 supplemented with 10% heat-inactivated FBS and 1% penicillin-streptomycin.

METHOD DETAILS

In vivo tumor growth

B16-F10 or CT26 cells, resuspended in PBS, were subcutaneously injected into the right flanks of male and female mice. TRAMP-C1 cells, dispersed in Matrigel, were subcutaneously injected into the right flanks of male mice only, as these prostate cancer cells demonstrate improved growth in male mice. Tumor growth was monitored every other day by measuring the width and length with a digital caliper. Tumor volume was calculated using the formula (width^2 x length)/2. The endpoint for tumor size was defined as when the tumor length reached 20 mm, at which point euthanasia was required.

Tumor growth in *Irf4*$^{fl/fl}$*Cd4-Cre vs.* WT mice

To investigate the effect of T cell-specific IRF4 deletion on syngeneic tumor growth, 0.1 x 10^6 B16-F10 melanoma cells or 2 x 10^6 TRAMP-C1 prostate cancer cells were subcutaneously injected into *Irf4*$^{fl/fl}$*Cd4-Cre* and WT B6 mice. B16-F10 bearing mice were sacrificed at 20 days post-tumor implantation for flow cytometry analysis, or when tumor length reached 20 mm. TRAMP-C1 bearing mice were sacrificed at 74 days post-tumor implantation. Additionally, to determine the impact of T cell-specific IRF4 deletion on allogeneic tumor growth, 1 x 10^6 CT26 colon carcinoma cells of Balb/c origin were subcutaneously injected into *Irf4*$^{fl/fl}$*Cd4-Cre*, WT BALB/c, and WT B6 mice.

Tumor processing for TIL analysis

To analyze tumor-infiltrating leukocytes (TILs), the B16-F10 tumors were minced and filtered through a 70 μM cell strainer to create a cell suspension. For the Tramp-c1 tumors, the tissue was minced with scissors and incubated with 400 U/mL collagenase IV and 30 U/ml DNase I at 37°C for 60 minutes, followed by filtration through a 70 μM cell strainer to generate a cell suspension. To enrich the TILs, red blood cells were lysed using ACK Lysing Buffer (Thermo Fisher Scientific), and the cell suspension was processed with Lympholyte-M (Cedarlane Laboratories) according to the manufacturer's instructions. The enriched TILs were then used for flow cytometric cell analysis or sorting.

Flow cytometry analysis

Splenocytes, cells in DLNs, TILs, and cultured T cells were stained and analyzed on an LSR II or Fortessa flow cytometer (BD Biosciences). Data was processed using FlowJo v10 software (Tree Star, Inc.). The fluorochrome-conjugated antibodies used for flow cytometry are listed in the key resources table. To exclude dead cells from analysis, the Zombie Aqua™ Fixable Viability Kit (BioLegend) was used. Intracellular expression of Ki-67 was determined using the Foxp3/Transcription Factor Staining Buffer Set (eBioscience) following the manufacturer's instructions. For intracellular staining of cytokines, *ex vivo* isolated T cells were re-stimulated with 50 ng/ml phorbol 12-myristate 13-acetate (Sigma-Aldrich) and 500 ng/ml ionomycin (Sigma-Aldrich) for 4 hours in the presence of GolgiStop (BD Biosciences). Cells were fixed and permeabilized using the Cytofix/Cytoperm™ solution (BD Biosciences) and then stained with fluorochrome-labeled antibodies against cytokines according to the manufacturer's instructions. For intracellular staining of IRF4, the IRF4 antibody (M-17, goat polyclonal IgG) was purchased from Santa Cruz Biotechnology, and the Donkey anti-Goat IgG (H+L) Secondary Antibody conjugated with Alexa Fluor 647 was purchased from Thermo Fisher Scientific. T cells were fixed and permeabilized using the Foxp3/Transcription Factor Staining Buffer Set (eBioscience), stained with the IRF4 antibody, and then stained with the Donkey anti-Goat IgG (H+L) Secondary Antibody.

Tracking *Irf4*$^{-/-}$ *vs.* WT Pmel-1 cells *in vivo*

To perform an adoptive transfer of freshly isolated Pmel-1 T cells, splenocytes were collected from Thy1.1$^+$ *Irf4*$^{-/-}$ Pmel-1 and Thy1.1$^+$Thy1.2$^+$ WT Pmel-1 mice. Red blood cells were lysed using ACK lysis buffer, and the splenocytes were mixed to create a 1:1 ratio of Thy1.1$^+$ *Irf4*$^{-/-}$ Pmel-1 and Thy1.1$^+$Thy1.2$^+$ WT Pmel-1 T cells. A total of 1 x 10^6 Thy1.1$^+$ *Irf4*$^{-/-}$ Pmel-1 and 1 x 10^6 Thy1.1$^+$Thy1.2$^+$ WT Pmel-1 T cells were injected intravenously into Thy1.2$^+$ WT B6 mice on the same day that 0.5 x 10^6 B16-F10 melanoma cells were injected subcutaneously.

To perform an adoptive transfer of activated Pmel-1 T cells, splenocytes from Thy1.1$^+$ *Irf4*$^{-/-}$ Pmel-1 or Thy1.1$^+$Thy1.2$^+$ WT Pmel-1 mice were stimulated with 1 μM hgp100$_{25\text{-}33}$ peptide and 10 ng/mL recombinant IL-2 in complete RPMI-1640, supplemented with 10% heat-inactivated FBS, 1% penicillin-streptomycin, and 0.1% 2-Mercaptoethanol. Two days after peptide stimulation, cultured splenocytes from both mouse groups were mixed to create a 1:1 ratio of activated Thy1.1$^+$ *Irf4*$^{-/-}$ Pmel-1 and Thy1.1$^+$Thy1.2$^+$ WT Pmel-1 T cells. A total of 1 x 10^6 Thy1.1$^+$ *Irf4*$^{-/-}$ Pmel-1 and 1 x 10^6 Thy1.1$^+$Thy1.2$^+$ WT Pmel-1 T cells were injected intravenously into Thy1.2$^+$ WT B6 mice on the same day that 0.5 x 10^6 B16-F10 melanoma cells were injected subcutaneously. On day 14 post B16-F10 implantation, the frequencies of transferred Pmel-1 T cells in spleens, DLNs, and tumors were determined by flow cytometry analysis.

Overexpressing IRF4 via retroviral transduction

The cDNA fragments encoding mouse *Irf4* were PCR amplified and inserted into a pMYs-IRES-EGFP retroviral vector (Cell Biolabs). The retroviral particles were generated by transfecting plat-E cells with the IRF4-GFP vector or the empty GFP-control vector, following the manufacturer's instructions (Cell Biolabs). To transduce IRF4-GFP or GFP-control retrovirus into Pmel-1 cells, splenocytes from Thy1.1$^+$ WT Pmel-1 mice were stimulated with 1 μM hgp100$_{25\text{-}33}$ peptide and 10 ng/mL recombinant IL-2 in complete RPMI-1640 medium supplemented with 10% heat-inactivated FBS, 1% penicillin-streptomycin, and 0.1% 2-Mercaptoethanol. After 24 hours of peptide stimulation, cultured splenocytes were incubated with freshly prepared retroviral particles by centrifugation for 2 hours at 780g and 32°C in the presence of 8 μg/mL

polybrene (Sigma-Aldrich). After centrifugation, the cells were first cultured for 6 hours at 32°C and then for an additional 24 hours at 37°C in complete RPMI-1640 medium before flow cytometry analysis and adoptive transfer of Pmel-1 cells.

ACT using IRF4-transduced Pmel-1 cells

Adoptive cell therapy (ACT) using IRF4-transduced Pmel-1 cells was employed to treat B16-F10 melanoma. Twenty-four hours following retroviral transduction of IRF4-GFP or GFP-control, flow cytometry analysis was used to determine the percentage of GFP-expressing cells in cultured Thy1.1$^+$ WT Pmel-1 T cells. Cultured cells containing 1 x 10^6 GFP$^+$ (either IRF4-GFP or GFP-control transduced) Pmel-1 T cells were adoptively transferred to Thy1.2$^+$ (or Thy1.2$^+$CD45.1$^+$) B6 mice on day 3 after subcutaneous injection of 0.5 x 10^6 B16-F10 cells. Tumor growth was monitored every other day. Additionally, on day 14 post B16-F10 implantation, some mice were sacrificed to perform flow cytometry and scRNA-Seq analysis of the adoptively transferred Pmel-1 T cells.

ScRNA-seq of Pmel-1 and endogenous TILs

ScRNA-seq was performed at the Single Cell Genomics Core at Baylor College of Medicine (Houston, TX). The Single Cell Gene Expression Library was prepared using the Chromium Next GEM Single Cell 3' Reagent Kits v3 (10x Genomics). Briefly, a single cell suspension, reverse transcription reagents, Gel Beads containing barcoded oligonucleotides, and oil were loaded onto a Chromium controller (10x Genomics) to generate single cell GEMs (Gel Beads-In-Emulsions), where full-length cDNA was synthesized and barcoded for each single cell. Subsequently, the GEMs were broken, and cDNA from each single cell was pooled. After cleanup using Dynabeads MyOne Silane Beads, the cDNA was amplified by PCR. The amplified product was fragmented to an optimal size before undergoing end-repair, A-tailing, and adaptor ligation. The final library was generated through amplification, and its quantity was determined using the KAPA Library Quantification kit (Roche). The libraries were then sequenced using a Novaseq 6000 (Illumina).

The Cell Ranger Single Cell Software Suite (v3.0.2) was used to perform bioinformatic analysis. The reads were aligned to the mouse transcriptome reference (mm10, Ensembl 93) with STAR.[39] Raw read count tables were analyzed using the Seurat (v3.0.1)[38] standard pipeline on the R platform (v3.6.0). We filtered out the cells with the percent.mt > 5 & nCount_RNA > 100000 & nFeature_RNA <= 200. FindVariableGenes function was used to calculate the top principal components. UMAP clusters of cells were identified based on the first ten principal components. Cell clusters were identified using the shared nearest neighbor algorithm[38] with a resolution parameter of 0.8. FindMarkers function was used to identify differentially expressed genes between cell groups using Wilcoxon Rank Sum test. Feature plots and Violin plots were displayed with the log (raw read count +1) of the gene/cell on UMAP embedding.

ACT using Pmel-1 cells plus PD-L1 blockade

To assess the effectiveness of IRF4-transduced Pmel-1 adoptive cell therapy (ACT) in combination with PD-L1 blockade against tumors, Thy1.2$^+$ B6 mice were subcutaneously injected with 0.5 x 10^6 B16-F10 cells. On day 3, the mice were adoptively transferred with cultured Pmel-1 splenocytes containing 1 x 10^6 GFP$^+$ Pmel-1 T cells (either IRF4-GFP or GFP-control transduced). The mice were then intraperitoneally injected with 200 μg of anti-PD-L1 mAb (clone 10F.9G2; Bio X Cell) on days 3, 6, and 9. Other groups of mice bearing B16-F10 tumors were treated with only anti-PD-L1 mAb or received no treatment. Tumor growth was monitored every other day.

QUANTIFICATION AND STATISTICAL ANALYSIS

Data were represented as mean ± SD and analyzed with Prism version 9.1.2 (GraphPad Software). Flow cytometry data analysis was performed using FlowJo Version 10 (Tree Star). The sample size for the animal experiments was determined based on the literature and our previous experience with similar experiments. Statistical significance of survival curves was analyzed using the log-rank test. Unpaired two-tailed Student's *t*-test was used for other measurements. Differences were considered significant when $p < 0.05$. p values are denoted in figures as follows: *$p < 0.05$, **$p < 0.01$, ***$p < 0.001$, and ****$p < 0.0001$.